An edge-driven 3D region-growing approach for upper airway morphology and volume evaluation in patients with Pierre Robin sequence

Carmelo Militello*

Istituto di Bioimmagini e Fisiologia Molecolare (IBFM CNR),
Consiglio Nazionale delle Ricerche,
Contrada Pietrapollastra-Pisciotto,
90015, Cefalù, PA, Italy
Email: carmelo.militello@ibfm.cnr.it
*Corresponding author

Salvatore Vitabile

Dipartimento di Biopatologia e Biotecnologie Mediche (DIBIMED),
Università degli Studi di Palermo,
Via del Vespro, 90127, Palermo, Italy
Email: salvatore.vitabile@unipa.it

Leonardo Rundo

Istituto di Bioimmagini e Fisiologia Molecolare (IBFM CNR),
Consiglio Nazionale delle Ricerche,
Contrada Pietrapollastra-Pisciotto,
90015, Cefalù, PA, Italy
Email: leonardo.rundo@ibfm.cnr.it

Cesare Gagliardo and Sergio Salerno

Dipartimento di Biopatologia e Biotecnologie Mediche (DIBIMED),
Università degli Studi di Palermo,
Via del Vespro, 90127, Palermo, Italy
Email: cesare.gagliardo@unipa.it
Email: sergio.salerno@unipa.it

Abstract: Pierre Robin sequence (PRS) is a pathological condition responsible for a sequence of clinical events, such as breathing and feeding difficulties, that must be addressed to give the patient at least a chance to survive. By using medical imaging techniques, in a non-intrusive way, the surgeon has the opportunity to obtain 3D views, reconstruction of the regions of interest (ROIs), useful to increase understanding of the PRS patient's condition. In this paper, a semi-automatic approach for segmentation of the upper airways is proposed. The implemented approach uses an edge-driven 3D region-growing algorithm to segment ROIs and 3D volume-rendering technique to reconstruct the 3D model of the upper airways. This method can be used to integrate information inside a medical decision support system, making it possible to

enhance medical evaluation. The effectiveness of the proposed segmentation approach was evaluated using Jaccard (92.1733%) and dice (94.6441%) similarity indices and specificity (96.8895%) and sensitivity (97.6682%) rates. The proposed method achieved an average computation time reduced by a 16x factor with respect to manual segmentation.

Keywords: 3D region growing; edge-driven segmentation; airway segmentation; Pierre Robin sequence; PRS; 3D modelling; medical decision support system; MDSS.

Reference to this paper should be made as follows: Militello, C., Vitabile, S., Rundo, L., Gagliardo, C. and Salerno, S. (2015) 'An edge-driven 3D region-growing approach for upper airway morphology and volume evaluation in patients with Pierre Robin sequence', *Int. J. Adaptive and Innovative Systems*, Vol. 2, No. 3, pp.232–253.

Biographical notes: Carmelo Militello received his Laurea and PhD in Computer Science Engineering from the University of Palermo, Italy, in 2006 and 2010, respectively. During his PhD course, he has been involved in medical and biometrics imaging and digital architecture development and implementation. Since 2011, he is a researcher of the Institute of Molecular Bioimaging and Physiology – Italian National Research Council (IBFM-CNR), Cefalù (PA) unit. His activity is also conducted in collaboration with the Department of Biopathology and Medical Biotechnologies, University of Palermo, Italy. His main research areas are in the field of the analysis and processing of medical images, with particular interest to MRgFUS treatment issues and Gamma Knife radio-surgery planning.

Salvatore Vitabile received his Laurea degree in Electronic Engineering and his Doctoral in Computer Science from the University of Palermo, Italy, in 1994 and 1999, respectively. He is currently an Assistant Professor with the Department of Biopathology and Medical Biotechnologies, University of Palermo, Italy. In 2007, he was a Visiting Professor in the Department of Radiology, Ohio State University, Columbus, USA. He has co-authored more than 150 scientific papers in referred journals and conferences. He has chaired, organised, and served as member of the organising committee of several international conferences and workshops. He is also a member of the board of directors of SIREN (Italian Society of Neural Networks). His research interests include specialised architecture design and prototyping, neural networks, biometric authentication systems, real-time driver assistance systems, and medical data processing.

Leonardo Rundo is currently working as a Research Fellow at Institute of Molecular Bioimaging and Physiology – Italian National Research Council (IBFM-CNR), Cefalù (PA) unit. He received his Bachelor and Master degrees in Computer Science Engineering from University of Palermo in 2010 and 2013, respectively. His main scientific research interests include digital image processing (in particular image segmentation and analysis), medical imaging, high intensity focused ultrasound and radiation therapy, human computer-interaction, automatic GUI generation applied to medical diagnostic software and e-Health.

Cesare Gagliardo graduated in Medicine and Surgery in 2006 at the University of Palermo; qualified as a Medical Doctor in 2007 and as a Radiologist in 2011. He received his PhD in Neuroscience and Behaviour Disorders since 2015. He has presented scientific papers at national and international conferences, participated in numerous courses and conferences, and, as a speaker, at some of

national and international conferences. Currently, he is in the research field as a Research Fellow at the Department of Radiological, Oncological and Anatomo-pathological Sciences Policlinico Umberto I (Sapienza University of Rome).

Sergio Salerno received his Medical degree in 1992 and completed the Specialist training in Radiology in Palermo University, Italy. He is a Research Fellow (CIRSE) in the Department of Diagnostic Radiology in St' Georges Hospital London, UK. He has a PhD in Diagnostic Radiology in Oncology in 2000. His research interests include radiation protection, diagnostic performance in CT and MR and computational elaboration of images obtained in different imaging modalities such as CT and MR. He published about 160 papers in refereed journals and international conference proceedings. He was invited speakers in about 50 national and international conferences. He has been a member of ESR European Society of Radiology CIRSE Cardiovascular and Interventional society of Europe and ESPR European Society of Paediatric Radiology and has served as the Chairman of the Section of Radiation protection and Radiobiology of the Italian Society of Radiology (SIRM).

1 Introduction

Pierre Robin malformation was first described in 1923 by the French surgeon Pierre Robin (1994).The exact cause of Pierre Robin malformation is not known, but it is thought to depend on something that, during the first gestational weeks, would interfere with the posterior-inferior sliding of the tongue that normally allows the sides of the palate to shift to the midline and close. The main investigated factor is the underdevelopment of the mandible that could be the result of an inherent (genetic or syndromic) or a secondary growth problem (high intrauterine pressure, oligohydramnios) (Carroll et al., 1971; Cohen, 1990; Jakobsen et al., 2006).Today this condition is recognised as a 'sequence' (Pierre Robin Sequence, PRS) because the underdeveloped mandible is responsible for a sequence of clinical events. The small or displaced mandible may also cause the tongue to be positioned at the back of the mouth, causing breathing and feeding difficulties (Schreiner et al., 1973).

There is no absolute indication to surgery for PRS patients. However, depending on the severity of respiratory impairment, surgery may be indicated to repair the cleft palate and correct the airway duct, to aid feeding and to improve breathing (Lidsky et al., 2008; Leboulanger et al., 2010). Controversies about the diagnosis and management of PRS are summarised in Mackay (2011). The possibility of measuring the volume of the upper airways to select patients eligible for surgery may be decisive for patient outcome: the proposed approach may help by giving an answer to this question.

In this scenario, medical imaging is useful to develop algorithms generating 3D volumetric reconstruction of the airways. Such reconstruction can provide an intuitive view of the upper airway structure, useful to integrate medical information during diagnosis and surgery evaluation processes.

This paper is organised as follows: Section 2 describes similar works in the literature; Section 3 illustrates the proposed 3D Region-Growing approach for upper airway segmentation and reconstruction; Section 4 shows and discusses the obtained experimental results; finally, Section 5 provides some discussions and conclusions about this work.

2 Related works

In literature there are several works dealing with the airway segmentation problem. However, almost always segmentation approaches are applied to healthy patients, in which ROIs have a morphology dominated by anatomical symmetries/similarities that, allowing the use of templates, simplify the identification and segmentation of the structures of interest.

Tan et al. (2012) propose an approach to segment the airway tree from multi-slice computed tomography (MSCT). In this approach, it is possible to locate three processing steps: in the first one, using an adaptive threshold algorithm, the seed-point for region-growing is extracted; in the second one, starting from the extracted seed-point, the segmentation of the main bronchi is performed using a 3D region-growing algorithm and, simultaneously, leakage points into the lung parenchyma are detected; finally, in the third one, the probable leakage points are selected using a simulation of 3D region-growing based on parallel computing.

Lin et al. (2006) try to reconstruct a 3D model of the nasal cavity, pharynx, larynx and trachea. The purpose of this study was to search for the effect of inhaled aerosols on the human upper airway. The obtained geometric reconstruction is an anatomically realistic model that derives from a computed tomography (CT) dataset of the whole respiratory tract of normal adults. Starting from the provided CT dataset, an accurate 3D model of the human upper airway is reconstructed.

Yousefi Rizi et al. (2008b) propose a fuzzy-based algorithm for 3D segmentation of the human airway. To overcome leakage problems outside the ROI during the segmentation process, a multi-seeded fuzzy-based region-growing approach in conjunction with the spatial information of voxels is proposed. In Yousefi Rizi et al. (2008a), the same authors propose an optimisation of their previous segmentation method, where a mathematical shape optimisation approach is used (based on a fuzzy connectivity algorithm) to preserve shape features of the object. The novelty of this proposed scheme is to prevent leakage rather than taking leak detection and leak reduction approaches.

Seo et al. (2010) implement a software tool for semi-automatic segmentation of the nasal airway. A 3D region-growing algorithm is used to perform the segmentation that provides, as a result, a 3D model. This approach is applied because the nasal airway can be recognised by grouping similar pixel values of respiratory paths from CT images. To visualise the 3D model of the nasal airway a volume rendering method is used.

Aykac et al. (2003) describe a fully automatic technique for segmenting the airway tree starting from 3D CT images of the thorax. Grey-scale morphological reconstruction is used to identify pixel candidates belonging to airways. After segmentation, 3D reconstruction of the airway tree and estimation of airway branch-points in the reconstructed tree are performed.

Bresch and Narayanan (2009) propose a method for unsupervised region segmentation of an image using its spatial frequency domain representation. The algorithm is designed to process large sequences of real-time magnetic resonance (MR) datasets containing the 2D mid-sagittal view of a human vocal tract airway. The segmentation algorithm uses an anatomical object model, whose fit to the observed image data is hierarchically optimised using a gradient descent procedure.

The segmentation of the upper airway in PRS patients may not be an easy task, because there are difficulties due to the almost total absence of symmetries and anatomical similarities with healthy patients that do not give the possibility to use models for segmentation. Moreover, restrictions on the radiation amount, given to patients with only a few months of life, limit the CT image resolution. This problem is particularly evident in PRS patients where the airways, presenting very small sections (caused by stenosis or by breathing movement), can become difficult or impossible to detect.

In this scenario, segmentation can be a complicated process with respect to healthy patients, making it impossible to identify correctly the airways. For this reason, a completely automated process is not always useable. This brings us to the need for a semi-automatic approach where a supervisor evaluates the particular situation and proceeds with the correct segmentation.

The use of medical imaging techniques is motivated by the need to provide a tool that assists the surgeon in the evaluation process of the PRS disease. Segmentation approaches fall into one of the following classes: thresholding, edge-detection, clustering, active contour, and region-growing. Techniques based on (global or dynamic) thresholding have the advantage of greater computational simplicity, but the results are not always so good. This leads to the need for further post-processing steps. Techniques based on edge-detection operators (such as Sobel or Canny) extract the contours associated with high gradient areas, sometimes obtaining opened boundaries, which are difficult to use for 3D reconstructions. More sophisticated edge-detection operators (such as Marr-Hilldreth) obtain closed boundaries, with the ROI over-segmentation drawback. Even techniques based on clustering are not always usable, because some parameters are not always available. For example, clustering based on k-means needs to know *a-priori* the number of clusters and such information is not always available. Another parameter to evaluate is the computational cost of the algorithm and its processing time. Active contour techniques [such as level-set function (LSF)] obtain good results in the segmentation process, and, however, may require more time for tuning of the various parameters and high processing time, related to not fast convergence.

Unlike previous techniques, approaches based on region-growing obtain well-defined ROIs with good processing time and rapid applicability because of the few parameters to be set. A problem of techniques based on region-growing is ‘leakage’, which is related to the growth of the region outside the ROI boundaries.

The approach described in this article is based on a 3D region-growing used to segment the ROIs on the entire dataset. The operator should only select the initial seed-point and the algorithm will proceed automatically with the growing process in all dataset slices. To prevent leakage, the region-growing process is aided by information provided by the difference in strength (DIS) map, which provides a measurement of the distance of the pixels from the ROI edge. Successively, with the segmented ROIs, the 3D anatomical model of the airways is reconstructed and visualised.

3 The proposed edge-driven 3D region-growing approach

This paper proposes an approach using a 3D region-growing (3D-RG) algorithm to segment ROIs and 3D volume-rendering (3D-VR) techniques to reconstruct and display the corresponding three-dimensional model of the upper airways. In order to help the pathological scenario assessment of the PRS patient and to correctly address possible corrective surgery (Kirschner et al., 2003), extracted information could be used in a medical decision support system (MDSS) to integrate medical data about the patient and to assist the surgeon in the disease evaluation phase.

Figure 1 The implemented GUI based on the proposed airway segmentation approach (see online version for colours)

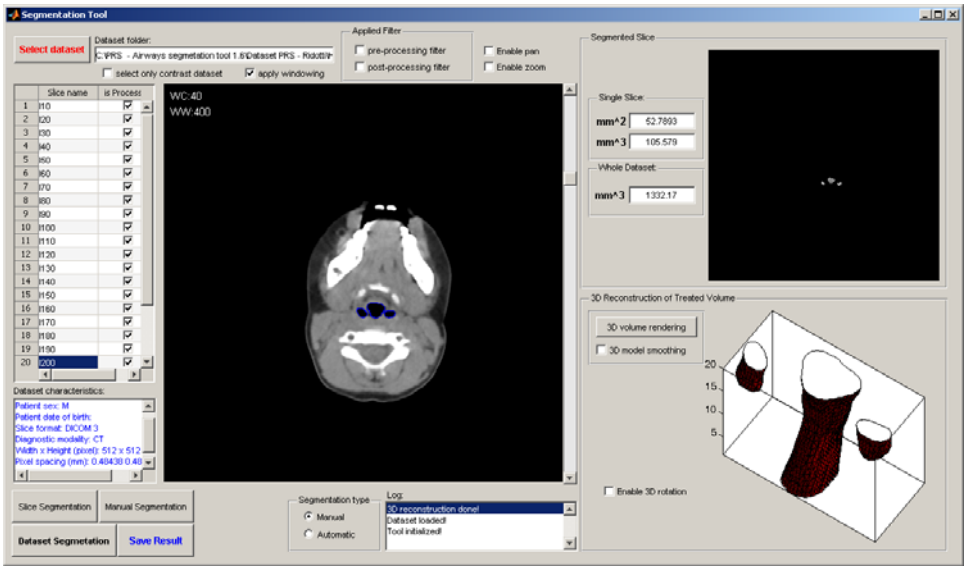

Notes: On the left side is the list and the dataset characteristics. In the centre is the selected slice. In the top-right corner is the mask with the segmented ROI and the corresponding surface and volume. In the lower-right corner is the reconstructed 3D model obtained after region-growing segmentation.

In particular, to work correctly the proposed 3D-RG approach needs

1 a threshold to locate the pixel range belonging to the ROI

2 an edge map, provided using DIS, to avoid growth beyond the airway boundaries.

After the region-growing phase, a 3D reconstruction is performed using the extracted ROIs. The computed 3D model is visualised with information about volume and surface. Making it possible to automatically calculate the upper airway volume and to easily obtain a 3D-VR model, the proposed approach can be used to provide the surgeon a means of support in the therapeutic path of the PRS patient.

As illustrated in Figure 1, the realised graphical user interface (GUI) provides all the necessary controls

1 to select a CT scan

2 to choose the slice of interest

3 to visualise the segmented area of each slice and to display the slice surface and the total volume of the airways.

The possibility to zoom/move the 3D model allows the operator to interact with the GUI and display details of the 3D-VR model from different points of view.

3.1 Approach description

Figure 2 shows the flow diagram of the processing steps realised with the proposed approach. It is possible to recognise the following steps:

- *region of treatment (ROT) identification*: the step where the operator selects the region from which the region-growing algorithm starts
- *region-growing threshold selection*: this step determines a threshold (using the Otsu method) used by the region-growing algorithm to establish whether to add the pixel to the ROI
- *DIS map calculation*: edge information is used to help the region-growing algorithm to process correct boundary pixels, avoiding leaking
- *edge-driven 3D region-growing*: starting from the seed-point, detected automatically inside the ROT, this step begins the growth including only the pixels that satisfy the region-growing conditions
- *surface and volume computation*: after the region-growing segmentation, this step determines the surfaces of each extracted ROI and the overall upper airway volume
- *3D airway model reconstruction*: starting from ROIs, a 3D model is build and visualised in the GUI to the operator.

Figure 2 Flow diagram of the processing steps performed in the implemented segmentation approach (see online version for colours)

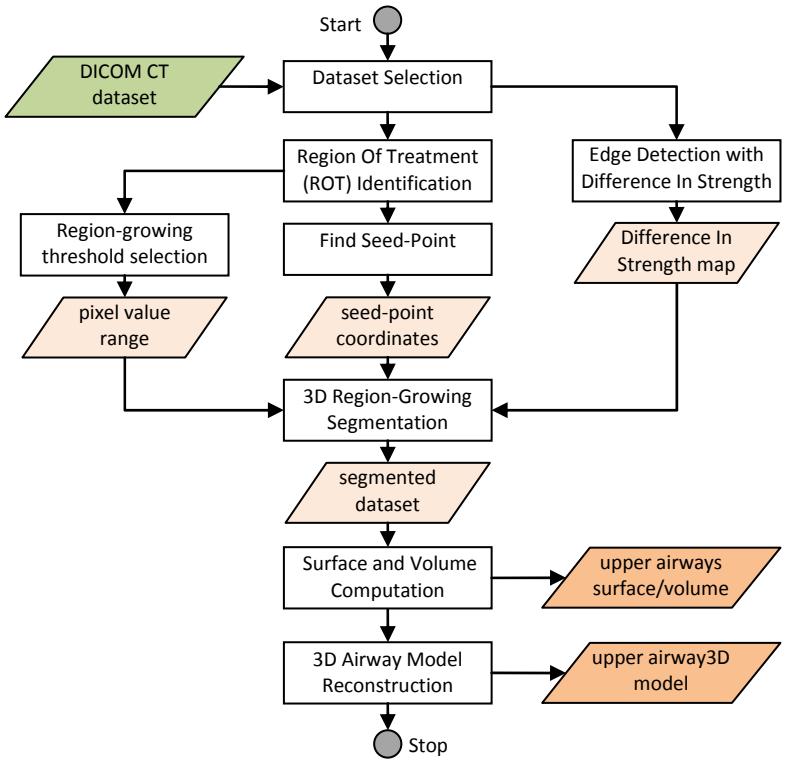

Figure 3 ROT identification, (a) initial CT slice (b) selection of initial ROT (c) starting from this ROT, the software locates the seed-point (see online version for colours)

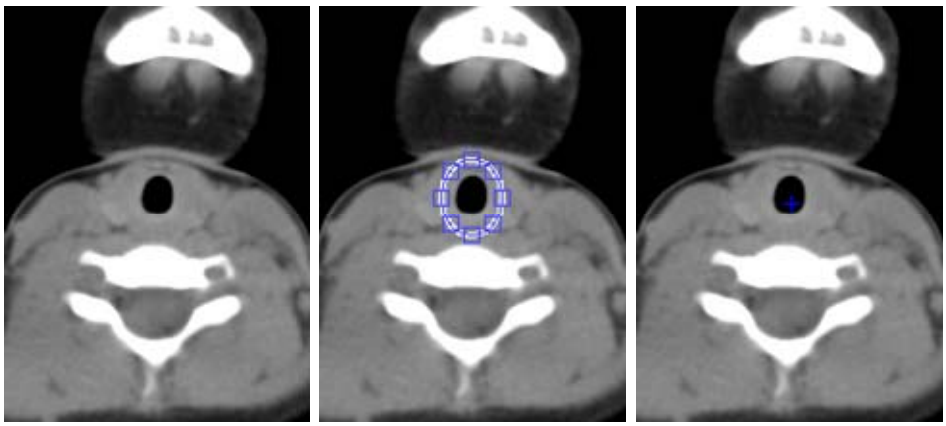

(a) (b) (c)

Note: The absolute minimum point is indicated with a blue cross.

3.1.1 ROT identification

As shown in Figure 3, before the region-growing algorithm starts, the operator must select the ROT, used for the segmentation and the extraction of ROIs [Figure 3(b)]. Within this ROT, the initial seed-point is identified, given by the absolute minimum point [Figure 3(c)]. It is possible to use this approach because in the CT images the air presents the lowest intensity pixel values. Depending on the particular morphology of the anatomical section considered, the realised GUI provides the possibility of various shapes for the selection of the ROT (e.g., elliptical, rectangular).

3.1.2 Region-growing threshold selection

In literature, there are some approaches where an absolute threshold of the pixel values is considered (Zhu et al., 2010). This approach is not always usable, in fact, images coming from different CT scanners may have not perfectly aligned pixel ranges, due to differences in the calibration process. Because of this, the same anatomical structures, from different datasets, may have different pixel values. The situation becomes more complex when the scanners are from different manufacturers. In this case, there may be present, as well as shifts in the pixel range, even different standardisation/normalisation procedures of the output pixel, due to different values of some DICOM parameters (*rescaleSlope* and *rescaleIntercept*). In particular, equation (1) shows the relationship existing between the stored values (*storedValue*) and the output value (*outputValue*) as a linear function of these two parameters. As can be seen in Table 2, the different datasets have different values of these parameters which would require (before the region-growing segmentation) different normalisation procedures of images in the pre-processing phase.

$$outputValue = rescaleSlope \times storedValue + rescaleIntercept \tag{1}$$

For this reason it was decided to follow a different approach: from the ROT highlighted in the previous step, a threshold using the Otsu algorithm (1979) was selected. It is possible to use this approach because the histogram has a bimodal distribution of ROT divisible into two areas (ROI and background). The choice of a dynamic threshold allows the handling of datasets from different CT scanners without particular problems, since the algorithm will adapt to the various conditions of the processed dataset.

3.1.3 Edge-driven 3D region-growing

Starting from the seed-point located inside the ROT, the 3D Region-Growing algorithm analyses the 26 neighbours of the current pixel (in blue in Figure 4). For each of these 26 neighbours we verified if the condition expressed by the equation (2) is satisfied. This relation is composed of 4 sub-conditions [equations (3), (4), (5), (6)], checking if:

a the pixel is inside the image

b the pixel has not already been added to the ROI

c the value of the pixel satisfies the condition on the threshold

d the pixel is not an edge pixel.

If all these sub-conditions are satisfied, then the pixel will be added to the ROI. In the following there is the pseudo-code of the region-growing algorithm:

1 start;

2 set the minimum point in the ROT as initial seed-point;

3 put the seed-point in the *candidatesList*;

4 let P be the first point in the *candidatesList*;

5 if P satisfies the *conditionRG*;
   a add P to the ROI;
   b remove P from the *candidatesList*;
   c add the 26 neighbours of P to the *candidatesList*;

6 if P does not satisfy the *conditionRG*;
   a remove P from the *candidatesList*;

7 if the *candidatesList* contains other points then return to step 4;

8 end;

Figure 4 The 3D region-growing approach (see online version for colours)

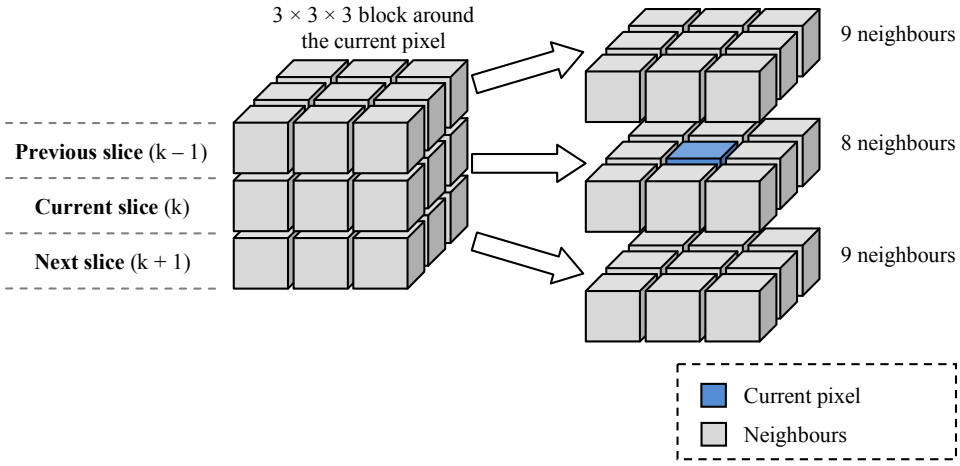

Notes: For each processed pixel (in blue in the centre) its 26-neighbourhood (in grey) is considered. These 26 neighbours are added to the *candidateList* and, subsequently, are added to the ROI only if all 4 sub-conditions [expressed by equations (3), (4), (5), (6)] are satisfied.

$$conditionRG(pixel(i,j)) = isInside(i,j) \,\&\, not(isInROI(i,j)) \,\&\, isInRange(pixel(i,j)) \,\&\, not(isEdgePixel(pixel(i,j))) \quad (2)$$

with:

$$isInside(i,j) = (0 \le i \le rows) \,\&\, (0 \le j \le columns) \quad (3)$$

$$isInROI(pixel(i,j)) = pixel(i,j) \in ROI \tag{4}$$

$$isInRange(pixel(i,j)) = pixel(i,j) \le thOtsu \tag{5}$$

$$\begin{aligned} isEdgePixel(pixel(i,j)) = [DIS(pixel(i,j)) > DIS(4neighbors(pixel(i,j)))] \\ \& [DIS(pixel(i,j)) > thDIS] \end{aligned} \tag{6}$$

In most cases the value of *thOtsu* is sufficient to properly segment the ROI, but when the edge is not well defined, the region-growing does not stop properly because of a not perfectly tuned *thOtsu* value. For this reason, ROI growth is also controlled by the DIS value associated with the pixels (Yu and Wang, 1999). The presence of condition (6) is justified by the need to avoid that the region-growing exceeds the ROI boundaries. The DIS map is calculated according to the equation (7), and highlights how the pixels are close to the boundary of the ROI (Figure 5). High values of DIS identify pixels near the edge of the ROI [Figures 6(a) and 6(b)]. Before a pixel *P*(i,j) is added to the ROI it is verified if

a the DIS exceeds the *thDIS* threshold [Figure 6(c)]

b the DIS is greater than the DIS values of its 4 neighbours: in this case the pixel will not be added to the ROI.

The use of the DIS map avoids leakage occurring in correspondence to the boundary with a low gradient. The most common edge-detection operators (e.g., Roberts, Prewitt, Sobel, etc.) are not always able to provide closed edges to manage the leaking phenomenon. The use of the map DIS improves the situation, practically without increasing the computational cost of the algorithm.

$$\begin{aligned} DIS(P(i,j)) = &|P_1 - P_3| + |P_1 - P_5| + |P_1 - P_6| + |P_1 - P_7| + |P_1 - P_8| + |P_2 - P_4| \\ &+ |P_2 - P_5| + |P_2 - P_6| + |P_2 - P_7| + |P_2 - P_8| + |P_3 - P_4| \\ &+ |P_3 - P_6| + |P_3 - P_7| + |P_3 - P_8| + |P_4 - P_5| + |P_4 - P_7| \\ &+ |P_4 - P_8| + \ldots |P_5 - P_6| + |P_5 - P_7| + |P_6 - P_8| \end{aligned} \tag{7}$$

Figure 5 Neighbour schemes used to calculate the DIS value associated with the P(i,j) pixel (see online version for colours)

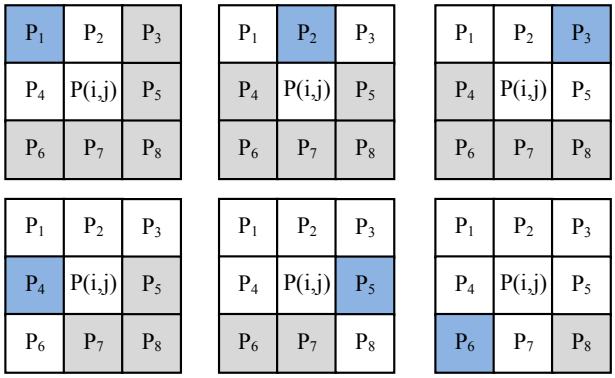

Notes: The DIS value is calculated considering the difference between the blue pixel and the corresponding grey pixels.

With more details, the method used to determine if a pixel is an edge-pixel is to compare its DIS with those of its 4-neighbouring inside a 3 × 3 window: if the DIS value of the pixel is the largest in both horizontal and vertical directions, then the pixel can be considered an edge-pixel. To avoid detecting false edge pixels, a *thDIS* threshold is used, to determine which pixels are truly located at the edges and which are not. The value of *thDIS* is set experimentally to 40% of the maximum value in the DIS map.

Figure 6 (a) example of a CT slice (b) the correspondent DIS map (c) 40% of max of the DIS map

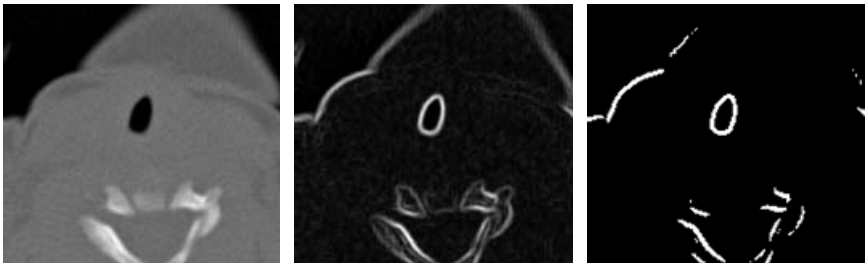

(a) (b) (c)

3.2 Airway volume computation

The volume of the segmented upper airways is calculated automatically considering the number of pixels belonging to the ROI extracted within each slice. The upper airway volume is evaluated using the following equations (8), (9) and (10).

$$airwayVolume = \sum_{k=1}^{n-1} volume(S_k, S_{k+1}) \tag{8}$$

with:

$$volume(S_k, S_{k+1}) = pixelCounter_k \times voxelVolume \tag{9}$$

$$voxelVolume = (pixelSpacingX \times pixelSpacingY) \times sliceThickness \tag{10}$$

where

- $volume(S_k, S_{k+1})$ is the volume between two consecutive slices S_k and S_{k+1}
- $pixelCounter_k$ is the number of pixels segmented in the slice S_k
- *sliceThickness* is the thickness between slices
- *pixelSpacingX* and *pixelSpacingY* are the spacing values between pixels along x and y axes.

3.3 Distinctive features

The proposed approach makes it possible to implement a semi-automatic method capable of segmenting the upper airways using a 3D region-growing approach. With the semi-automatic approach realised, the only human intervention is the ROT selection.

Errors in the segmentation process, due to leakage outside ROI boundaries, are avoided using DIS map information to enhance region-growing process. This segmentation modality may be used with some PRS patients where laryngo-pharyngeal channel morphology is not well defined and where basic region-growing might have some problems.

In the diagnosis phase, the obtained 3D-VR model, reconstructed with segmented ROIs, provides a view of laryngo-pharyngeal duct morphology giving additional information to improve understanding of the disease severity. This method, integrated with an MDSS, can help to support medical decision in clinical evaluation of PRS patients. The contribution of 3D models may also aid in the planning phase of any corrective surgery.

4 Experimental results

In this section the obtained experimental results, in terms of segmentation accuracy and 3D model reconstruction, are described. The proposed segmentation approach is evaluated using Jaccard (1901) and Dice (1945) similarity indices and sensitivity and specificity rates. Before the CT datasets used are described, showing some examples of images from datasets of patients with and without PRS.

4.1 Materials

The implemented approach was tested on 3 patients with isolated PRS with severe respiratory impairment, confirmed on clinical evaluation by laboratories tests and 2 controls not affected by craniofacial anomalies but with similar age, sex and weight, underwent a craniofacial and neck multi detector computed tomography (MDCT) 2D study (Table 1). Fortunately, PRS is a very rare disease (Bush and Williams, 1983; Printzlau and Andersen, 2004) and, consequently, also the availability of datasets on which to test the approach was very limited. During MDCT dataset acquisition, to avoid general anaesthesia and related tracheal intubation, young patients were subjected only to a mild sedation and thus CT studies were not acquired with a respiratory synchronised protocol and, of course, it was not possible to acquire breath-hold datasets. Our segmentation results were obtained considering the slices between palatine bone and vocal cords as anatomical landmarks.

Table 1 Information about the 2 controls and the 3 PRS patients

Dataset	*Gender*	*Age (days)*	*Weight (g)*
Healthy 1	Male	100	2,710
Healthy 2	Female	35	2,170
Pathological 1	Male	84	2,500
Pathological 2	Female	40	2,430
Pathological 3	Male	80	2,370

The 3 patients with PRS underwent an MDCT examination for a preliminary evaluation of upper airway calibre, in association with other cranial malformation and for the eventual surgical indication, whereas the 2 controls underwent an MDCT examination for

different clinical indications. MDCT scans where performed with the specifications shown in Tables 2 and 3.

Table 2 Characteristics and parameters of the MDCT datasets used

Dataset	*CT scanner*	*RescaleSlope values*	*RescaleIntercept values*	*Background value padding*	*Pixel range values*
Healthy 1	GE Hi Speed NX/i	1	0	–1,500	–1,122 ÷ 2,981
Healthy 2	Philips Brilliance	1	–1,024	no padding	–1,024 ÷ 2,329
Pathological 1	GE Hi Speed NX/i	1	0	–1,500	–1,190 ÷ 1,844
Pathological 2	GE Hi Speed NX/i	1	0	–1,500	–1,253 ÷ 4,000
Pathological 3	GE BrightSpeed 16	1	–1,024	–3,024	–1,024 ÷ 3,071

Note: It is possible to note different values obtained from the different CT scanners.

Table 3 Some characteristics of the CT dataset images used to test the proposed segmentation approach

Dataset	*Matrix size (pixel)*	*Pixel spacing (mm)*	*Slice thickness (mm)*
Healthy 1	512 × 512	0.4844	2
Healthy 2	512 × 512	0.2793	0.9
Pathological 1	512 × 512	0.3516	2
Pathological 2	512 × 512	0.3476	2
Pathological 3	512 × 512	0.2930	1.25

Figure 7 Example of CT slices of a patient without PRS

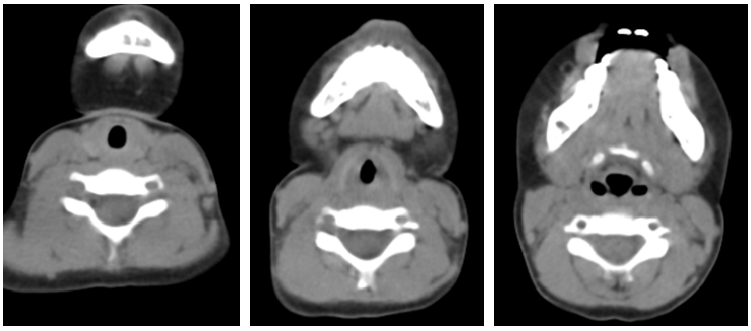

(a) (b) (c)

Notes: The course of laryngo-pharyngeal sections of the channel is very regular, the symmetries are respected and the edges are evident and well defined.

In patients without PRS, sections of the laryngo-pharyngeal tract had a regular pattern with an appreciable size (Figure 7), whereas in patients with PRS it was easy to see that the upper airway tract sections had a very irregular pattern and a reduced cross section [some clinical cases show a severe stenosis, as shown in Figure 8(c)].

Figure 8 Example of CT slices of a PRS patient

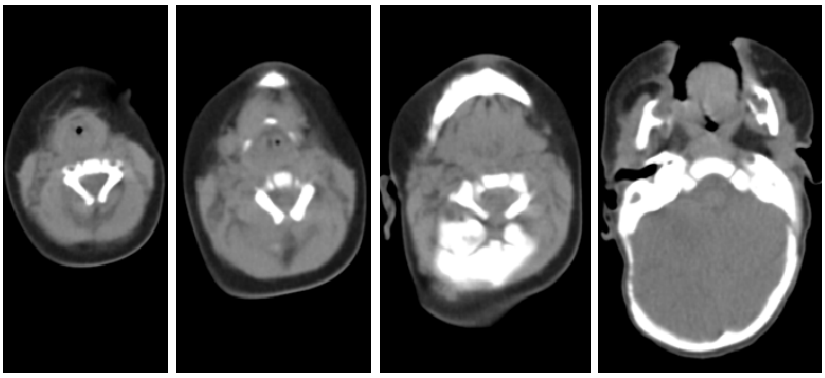

(a) (b) (c) (d)

Notes: The section of the laryngo-pharyngeal channel has a very irregular morphology. As can be seen in the c) images, the airway section even disappears, due to a severe stenosis.

Figure 9 Outcome of region-growing segmentation performed on healthy datasets, (a, d) the original CT slice (b, e) detail of upper airways and (c, f) detail of the segmented upper airway ROI

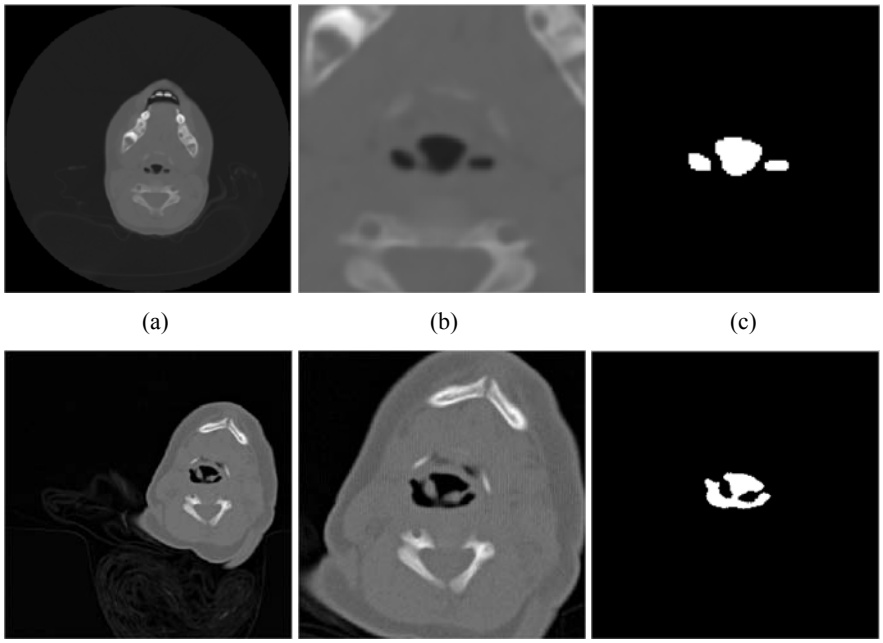

(a) (b) (c)

(d) (e) (f)

Figure 10 Outcome of region-growing segmentation performed on pathological datasets, (a,d) the original CT slice (b,e) detail of upper airways and (c,f) detail of the segmented upper airway ROI

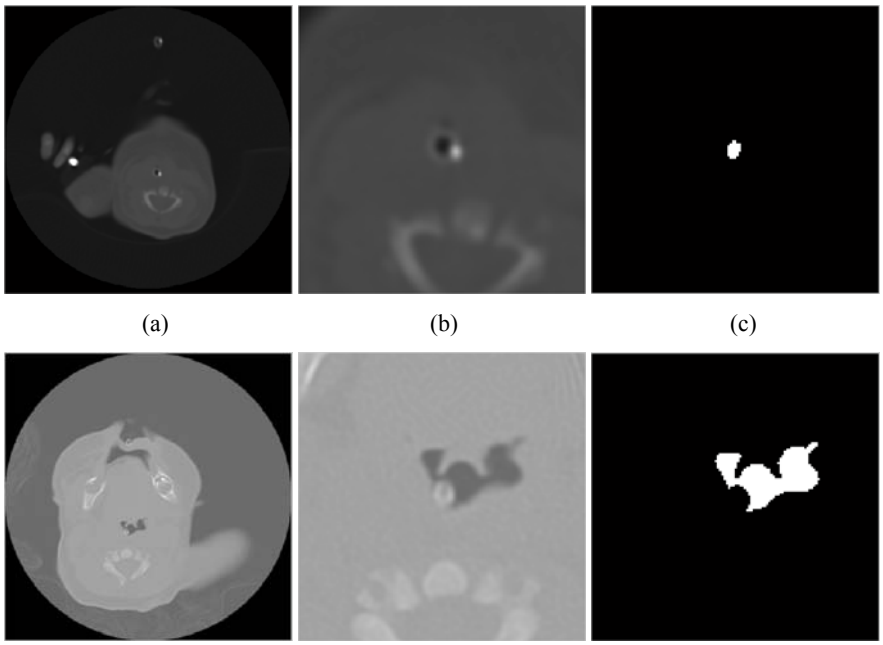

(a) (b) (c)

(d) (e) (f)

Figure 11 Slice of a PRS patient (pathological 1), (a) very small section of the Laryngo-pharyngeal tract (b) segmented ROI (c) zoomed segmented ROI (see online version for colours)

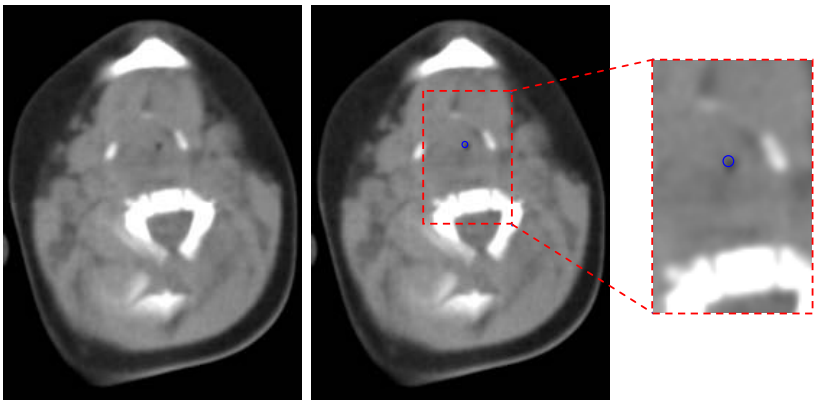

(a) (b) (c)

4.2 Segmentation evaluation

For the segmentation and extraction of the ROIs a 3D-RG algorithm was used, starting from a seed-point located inside a ROI selected by the operator. The region-growing

selects pixels that have an 'affinity' with the seed-point inside the selected ROI. The following figures show some examples of segmented ROIs from healthy (Figure 9) and pathological (Figures 10 and 11) datasets. Figure 11 shows a pathological dataset with particularly evident stenosis, correctly segmented using DIS map information, but that the basic region-growing could not segment.

The evaluation of the proposed segmentation approach was performed by calculating the Jaccard (1901) and Dice (1945) similarity indices, according to the equations (11) and (12). Sensitivity and specificity rates were also evaluated, according to equations (13) and (14). In order to calculate the above indices/rates, the results obtained with the proposed region-growing approach were compared with a manual segmentation performed by an experienced radiologist.

$$JaccardIndex(N_M, N_A) = \frac{|N_M \cap N_A|}{|N_M \cup N_A|} \tag{11}$$

$$DiceIndex(N_M, N_A) = \frac{2|N_M \cap N_A|}{|N_M| + |N_A|} \tag{12}$$

$$Sensitivity = \frac{N_{T_p}}{|N_M|} \tag{13}$$

$$Specificity = 1 - \frac{N_{F_p}}{|N_A|} \tag{14}$$

where

- N_M is the area manually segmented by the radiologist
- N_A is the segmented area with the proposed approach
- N_{T_p} is the number of true positive voxels
- N_{F_p} is the number of false positive voxels.

Table 4 shows the mean values of the Jaccard/Dice indices and the sensitivity/specificity rates. As already mentioned above, all these indices/rates were evaluated considering manual segmentation (performed by a radiologist) vs. the proposed semi-automatic segmentation approach.

In this imaging scenario, sensitivity (also called true positive rate) measures the proportion of positive pixels (belonging to the airways) which are correctly identified as such. Similarly, specificity (also called true negative rate) measures the proportion of negatives pixels (not belonging to the airways) which are correctly identified as such. Mean values of the Jaccard and Dice indices were 92.1733% and 94.6441%, while mean values of specificity and sensitivity rates were 96.8895% and 97.6682%. These results show good performance of the proposed segmentation approach based on the 3D region-growing.

Table 4 Jaccard/dice similarity indices and sensitivity/specificity rates obtained in the segmentation tests performed on 5 MDCT datasets

Dataset	*Jaccard index (%) (mean value ± SD)*	*Dice index (%) (mean value ± SD)*	*Specificity (%) (mean value ± SD)*	*Sensitivity (%) (mean value ± SD)*
Healthy 1	92.8255 ± 0.042	96.2314 ± 0.024	94.3931 ± 0.061	97.8028 ± 0.017
Healthy 2	92.7722 ± 0.025	96.2339 ± 0.014	95.8666 ± 0.030	96.5683 ± 0.025
Pathological 1	84.5148 ± 0.026	85.5632 ± 0.013	98.6336 ± 0.020	99.1434 ± 0.013
Pathological 2	97.6948 ± 0.034	98.8055 ± 0.018	99.0383 ± 0.026	98.5644 ± 0.018
Pathological 3	93.0590 ± 0.027	96.3861 ± 0.014	96.5161 ± 0.026	96.2617 ± 0.023

Table 5 shows the comparison of airway volumes obtained considering manual segmentation and the proposed 3D region-growing segmentation. It also shows the percentage difference between the two volumes.

Table 6 shows the processing times obtained by the proposed 3D-RG approach compared with the manual segmentation. These times, calculated using the MATLAB Profiler tool, refer to the complete execution of the implemented airway segmentation approach, running on a general-purpose Intel P4@3.2GHz (equipped with 2GB-DDR333 RAM). In the evaluation of these times the whole process was considered: from the selection of the ROT to the visualisation of the 3D model obtained from the segmented ROIs. For times related to manual segmentation, *'tic'* and *'toc'* MATLAB functions were used to measure elapsed time. From the comparison of the processing times it is possible to see an average reduction of the processing time by a 16x factor with respect to manual segmentation times.

Table 5 Airway volume comparison between manual segmentation and the 3D region-growing approach

Dataset	*Segmented volume with manual approach (mm^3)*	*Segmented volume with RG approach (mm^3)*	*Difference between manual and RG approaches (%)*
Healthy 1	332.82	343.21	+3.12
Healthy 2	276.05	268.44	–2.76
Pathological 1	261.28	271.12	+3.77
Pathological 2	193.14	198.65	+2.85
Pathological 3	135.77	133.47	–1.69

Table 6 Processing time required for ROI segmentation and the 3D airways model reconstruction

Dataset	*Number of processed slices*	*Reconstruction time of manual approach (s)*	*Reconstruction time of RG approach (s)*
Healthy 1	30	391.74	23.59
Healthy 2	27	327.56	28.16
Pathological 1	18	345.21	16.92
Pathological 2	20	296.04	17.39
Pathological 3	23	315.63	20.03

Figure 12 Three different views of the 3D model reconstruction obtained after segmentation of a control dataset, (a) panoramic view (b) sagittal view (c) coronal view (see online version for colours)

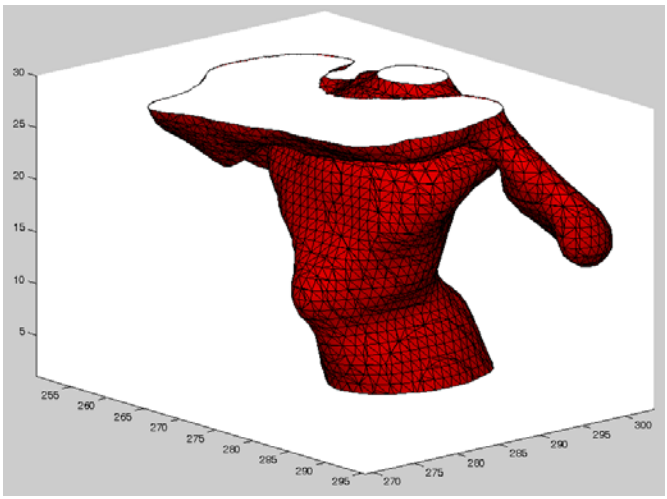

(a)

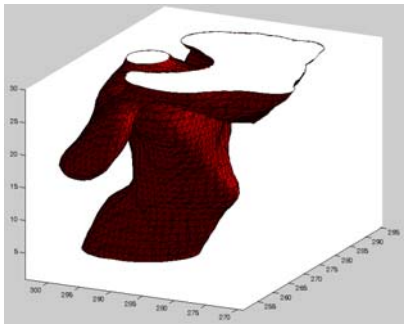

(b)

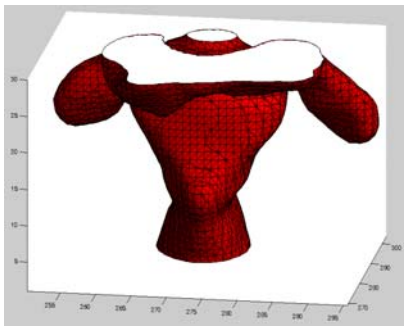

(c)

Figure 13 Three different views of 3D model reconstruction of a PRS patient, (a) panoramic view (b) sagittal view (c) coronal view (see online version for colours)

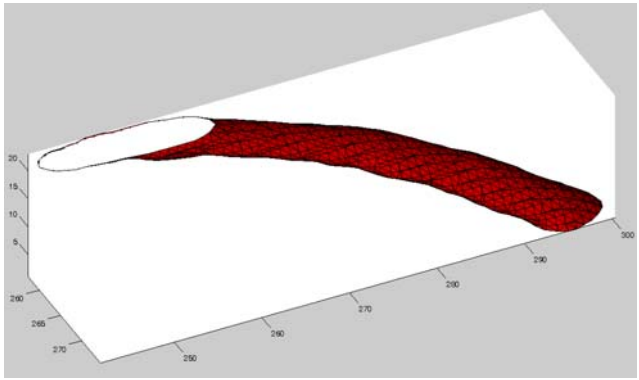

(a)

Figure 13 Three different views of 3D model reconstruction of a PRS patient, (a) panoramic view (b) sagittal view (c) coronal view (continued) (see online version for colours)

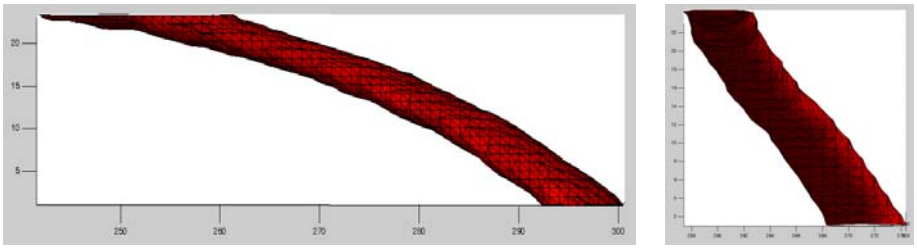

(b) (c)

4.3 3D volume reconstruction results

Segmented ROIs were used to reconstruct a three-dimensional model of airways channel using 3D-VR techniques. The obtained model gave a panoramic view of the Laryngo-pharyngeal tract morphology and provided useful information about the disease severity, useful in helping the assessment of surgical planning. After ROI segmentation, there are three processing steps to obtain the 3D model:

- *isosurface extraction*: isosurfaces are constructed from the ROIs extracted in the region-growing operation.
- *isosurface approximation with polygons*: a set of polygons (triangles) approximating the previously built isosurface is generated. In this phase specific colour characteristics can be assigned to the generated polygons.
- *normal surface to the isosurface computation*: this step, starting with the isosurface, determines the normal surface at the top of the isosurface. The aim is to achieve a more soft surface, thus avoiding the 'edginess' of the polygon surface.

The last step is to display the three-dimensional model generated by the insertion of some virtual illumination sources, in order to better visualise the effects. Figure 12 shows the 3D reconstruction of a control patient, while Figure13 shows an example of a PRS patient 3D reconstruction.

5 Discussion and conclusions

Morphological evaluation of upper airways is a key point in PRS patients. The risk of spontaneous desaturation episodes or asphyxiation during feeding or sleeping requires a careful monitoring of these young patients. Even if medical consensus exists for treating mild cases (with prone positioning alone) or for treating severe cases with tracheotomy (with subglottic obstructions), there is still a wide-open controversy about whether and how many of the remaining mild cases will have a catch-up growth of the underdeveloped mandible.

In this study an approach for semi-automatic segmentation of the upper airways has been proposed. The method uses an edge-driven 3D-RG algorithm to segment ROIs and 3D-VR techniques to reconstruct and display the corresponding 3D model of the upper

airways. This method, providing anatomical three-dimensional views and information about surface/volume, can be used to integrate information of an MDSS, making it possible to enhance and to help the effectiveness of the medical evaluation of the PRS disease.

MDCT studies, used in our segmentation tests, are not acquired with a synchronised respiratory protocol, since young patients are subject only to a mild sedation during acquisition and, of course, it is not possible to acquire breath-hold datasets. Because of this, datasets can have artefacts mainly caused by patient movement, such as accentuated stenosis caused by breathing. This can result in variability of upper airway calibre that is reflected in inaccurate data of the actual airway calibre and volume: this represents a limitation of our study. The second limitation of our study is the small population used, because of the low incidence of PRS (Bush and Williams, 1983; Printzlau and Andersen, 2004). Considering this, our study should be considered a concept proof. The only way to avoid this limitation is to include our approach in a multicentre study, in order to have a greater number of datasets and to obtain more robust statistical results. Even with these limitations, our approach represents a very easy way to make an initial quantitative evaluation of airway volume and to provide 3D reconstructions for surgeons who, usually, prefer to have a panoramic view of the anatomical site that they are going to treat.

Similarity indices and sensitivity/specificity rates were used to evaluate the accuracy of the proposed segmentation approach. In particular, mean values of the Jaccard and Dice indices were 92.1733% and 94.6441%, while mean values of specificity and sensitivity rates were 96.8895% and 97.6682% respectively. These measures show good performance of the proposed edge-driven region-growing approach. Moreover, our method obtained a processing time reduced by a 16x factor with respect to manual segmentation times.

References

Aykac, D., Hoffman, E.A., McLennan, G. and Reinhardt, J.M. (2003) 'Segmentation and analysis of the human airway tree from three-dimensional X-ray CT images', *IEEE Transactions on Medical Imaging*, Vol. 22, No. 8, pp.940–950, DOI: 10.1109/TMI.2003.815905.

Bresch, E. and Narayanan, S. (2009) 'Region segmentation in the frequency domain applied to upper airway real-time magnetic resonance images', *IEEE Transactions on Medical Imaging*, Vol. 28, No. 3, pp.323–338, DOI: 10.1109/TMI.2008.928920.

Bush, P.G. and Williams, A.J. (1983) 'Incidence of the Robin Anomalad (Pierre Robin syndrome)', *Br. J. Plast. Surg.*, Vol. 36, No. 4, pp.434–437.

Carroll, D.B., Peterson R.A., Worton E.W. and Birnbaum, L.M. (1971) 'Hereditary factors in the Pierre Robin syndrome', *Br. J. Plast. Surg.*, Vol. 24, pp.43–47, DOI: 10.1016/S0007-1226(71)80008-5.

Cohen Jr., M.M. (1990) 'Dysmorphology, syndromology and genetics', in McCarthy, J.G. (Ed.): *Plastic Surgery*, pp.69–112, WB Saunders, Philadelphia.

Dice, L.R. (1945) 'Measures of the amount of ecologic association between species', *Ecology*, Vol. 26, No. 3, pp.297–302.

Jaccard, P. (1901) 'Distribution de la florine alpine dans la Bassin de Dranses et dans quelques regiones voisines', *Bulletin de la Societe Vaudoise des Sciences Naturelles*, Vol. 37, pp.241–272.

Jakobsen, L.P., Knudsen, M.A., Lespinasse, J., García Ayuso, C., Ramos. C., Fryns, J.P., Bugge, M. and Tommerup, N. (2006) 'The genetic basis of the Pierre Robin sequence', *Cleft Palate Craniofac J.*, Vol. 43, No. 2, pp.155–159.

Kirschner, R.E., Low, D.W., Randall, P., Bartlett, S.P., McDonald-McGinn, D.M., Schultz, P.J., Zackai, E.H. and LaRossa, D. (2003) 'Surgical airway management in Pierre Robin sequence: is there a role for tongue-lip adhesion?', *Cleft Palate Craniofac J.*, Vol. 40, No. 1, pp.13–18.

Leboulanger, N., Picard, A., Soupre, V., Aubertin, G., Denoyelle, F., Galliani, E., Roger, G., Garabedian, E.N. and Fauroux, B. (2010) 'Physiologic and clinical benefits of non-invasive ventilation in infants with Pierre Robin sequence', *Pediatrics*, Vol. 126, No. 5, pp.e1056–e1063, DOI: 10.1542/peds.2010-0856.

Lidsky, M.E., Lander, T.A. and Sidman, J.D. (2008) 'Resolving feeding difficulties with early airway intervention in Pierre Robin sequence', *Laryngoscope*, Vol. 118, No. 1, pp.120–123.

Lin, J., Hu, G., Shen, H. and Fan, J. (2006) 'Three-dimensional reconstruction of the human upper airway from computed tomography images', *7th International Conference on Computer-Aided Industrial Design and Conceptual Design (CAIDCD'06)*, pp.1–5, DOI: 10.1109/CAIDCD.2006.329347.

Mackay, D.R. (2011) 'Controversies in the diagnosis and management of the Robin sequence', *J. Craniofac. Surg.*, Vol. 22, No. 2, pp.415–420, DOI: 10.1097/SCS.0b013e3182074799.

Otsu, N. (1979) 'A threshold selection method from gray-level histograms', *IEEE Transactions on Systems, Man, and Cybernetics*, Vol. 9, No. 1, pp.62–66, DOI: 10.1109/TSMC.1979.4310076.

Printzlau, A. and Andersen, M. (2004) 'Pierre Robin sequence in Denmark: a retrospective population-based epidemiological study', *Cleft Palate Craniofac J.*, Vol. 41, No. 1, pp.47–52.

Robin, P. (1994) 'A fall of the base of the tongue considered as a new cause of nasopharyngeal respiratory impairment: Pierre Robin sequence, a translation. 1923', *Plast. Reconstr. Surg.*, Vol. 93, No. 6, pp.1301–1303, DOI: 10.1097/00006534-199405000-00032.

Schreiner, R.L., McAlister, W.H., Marshall, R.E. and Shearer, W.T. (1973) 'Stickler syndrome in a pedigree of Pierre Robin syndrome', *Am. J. Dis. Child.*, Vol. 126, No. 1, pp.86–90.

Seo, A., Chung, S.K., Lee, J., Kim, J.I. and Kim, H.S. (2010) 'Semiautomatic segmentation of nasal airway based on collaborative environment', *Proocedings of the 2010 International Symposium on Ubiquitous Virtual Reality (ISUVR)*, pp.56–59, DOI: 10.1109/ISUVR.2010.24.

Tan, W., Yang, J., Zhao, D., Ma, S., Qu, L. and Wang, J. (2012) 'A novel method for automated segmentation of airway tree', *24th Chinese Control and Decision Conference (CCDC)*, pp.976–979, DOI: 10.1109/CCDC.2012.6244152.

Yousefi Rizi, F., Ahmadian, A., Fatemizadeh, E. and Alirezaie, J. (2008a) 'An optimization based approach embedded in a fuzzy connectivity algorithm for airway tree segmentation', *30th Annual International Conference of the IEEE Engineering in Medicine and Biology Society, (EMBS 2008)*, pp.4011–4014, DOI: 10.1109/IEMBS.2008.4650089.

Yousefi Rizi, F., Ahmadian, A., Sahba, N., Tavakoli, V., Alirezaie, J., Fatemizadeh, E. and Rezaie, N. (2008b) 'A hybrid fuzzy based algorithm for 3d human airway segmentation', *The 2nd International Conference on Bioinformatics and Biomedical Engineering (ICBBE 2008)*, pp.2295–2298, DOI: 10.1109/ICBBE.2008.906.

Yu, Y.W. and Wang, J.H. (1999) 'Image segmentation based on region growing and edge detection', *Proceedings of the IEEE International Conference on Systems, Man, and Cybernetics (IEEE SMC '99)*, Vol. 6, pp.798–803, DOI: 10.1109/ICSMC.1999.816653.

Zhu, C., Qi, S., van Triest, H., Wang, S., Kang, Y. and Yue, Y. (2010) 'Automatic 3D segmentation of human airway tree in CT image', *3rd International Conference on Biomedical Engineering and Informatics (BMEI)*, Vol. 1, pp.132–136, DOI: 10.1109/BMEI.2010.5639658.